ELSEVIER

Journal of Nuclear Materials 264 (1999) 283–294

journal of nuclear materials

A mechanism for the hydrogen uptake process in zirconium alloys

B. Cox *

Faculty of Applied Science and Engineering, Centre for Nuclear Engineering, University of Toronto, 184 College Street, Toronto, ON M5S 3E4, Canada

Received 2 January 1998; accepted 3 August 1998

Abstract

Hydrogen uptake data for thin Zircaloy-2 specimens in steam at 300–400°C have been analysed to show that there is a decrease in the rate of uptake with respect to the rate of oxidation when the terminal solid solubility (TSS) of hydrogen in the metal is exceeded. In order for TSS to be reached during pre-transition oxidation a very thin 0.125 mm Zircaloy sheet was used. The specimens had been pickled initially removing all Zr_2(Fe/Ni) particles from the initial surfaces, yet the initial hydrogen uptake rates were still much higher than for Zircaloy-4 or a binary Zr/Fe alloy that did not contain phases that dissolve readily during pickling. Cathodic polarisation at room temperature in $CuSO_4$ solution showed that small cracks or pores formed the cathodic sites in pre-transition oxide films. Some were at pits resulting from the initial dissolution of the Zr_2(Fe/Ni) phase; others were not; none were at the remaining intermetallics in the original surface. These small cracks are thought to provide the ingress routes for hydrogen. A microscopic steam starvation process at the bottoms of these small cracks or pores, leading to the accumulation of hydrogen adjacent to the oxide/metal interface, and causing breakdown of the passive oxide forming at the bottom of the flaw, is thought to provide the mechanism for the hydrogen uptake process during both pre-transition and post-transition oxidation.

1. Introduction

Investigators [1,2] continue to propose that hydrogen enters zirconium alloys during oxidation in aqueous environments by diffusing through the ZrO_2 lattice (or crystallite boundaries) of an impervious barrier oxide film. The intermetallic particles (in the Zircaloys) are seen as providing a direct short-circuit route for this process. This situation continues despite the accumulating evidence [3–5] that attempts to measure hydrogen diffusion in zirconia [6–10] are flawed. These attempts have usually followed one of two routes; implanting a hydrogen isotope in a preformed oxide and then measuring changes in the peak shape by a nuclear reaction [6–8] or measuring SIMS profiles of hydrogen species in oxides when the hydrogen isotope in the water is changed from H to D (and vice-versa) [3,9,10].

In the first type of experiment the authors found, for both Zircaloy-2 and Zr-2.5%Nb, that the hydrogen peaks tended to diminish in area without broadening during subsequent anneals, and sometimes became asymmetrical. Thus, even though the oxides were thin ($\leqslant 2$ μm), it was evident that migration to and escape down pores was the primary process occurring. To evaluate a diffusion coefficient from these results it was arbitrarily assumed that the pore spacing was 0.4 μm, despite electron microscope evidence for a much closer spacing in the columnar oxides that are typical of oxides of this thickness [11–13]. Asymmetries in the peaks which might have been indicative of radiation damage during implantation were ignored. Hence, diffusion coefficients calculated from these experiments should be regarded as unreliable, and biassed in the high direction.

The diffusion experiments based on successive SIMS profiling were shown not to follow the behaviour expected for a diffusion process in the oxide film [3]. More recent work [4] has clearly demonstrated that these experiments were measuring a rapid exchange process in

* Tel.: +1-416 978 2127; fax: +1-416 978 4155.

0022-3115/99/$ – see front matter
PII: S0022-3115(98)00492-9

the oxide film; that H/D, $^{6}Li/^{7}Li$ and $^{10}B/^{11}B$ all exchanged quantitatively and rapidly, and that all these species were probably adsorbed on pore walls within the oxide. Thus, the profiles obtained in these experiments represent the distribution of pore surface area through the thickness of the oxide. When all the species there initially (eg. OH^-) had exchanged for OD^- the deuterium profiles ceased to propagate. There is, therefore, no acceptable value for the hydrogen diffusion coefficient in a typical impervious ZrO_2 film available for comparison with results for hydrogen uptake rates during pre-transition oxidation kinetics.

Evidence for the direct involvement of the intermetallics as short-circuit paths for hydrogen ingress is based either on correlations of hydrogen uptake by the metal with particle sizes and distributions that have been modified by heat treatment [2], or with the observation (usually by tritium autoradiography at room temperature) of hydrogen concentrations in the intermetallic particles [14]. The first argument falls into the same trap that beset earlier work [15,16]. That is the belief that a correlation between hydrogen uptake and the chemistry or morphology of the precipitates implies their direct involvement in the process. It is known now that the intermetallic particles have a major effect on the oxide morphology (crack; pore development) and on the crystallite phases present in their vicinity [17–20]. Thus, the hydrogen may pass incidentally through the intermetallic particle, but it would be the cracks or pores in the oxide that the intermetallic stimulated rather than any high diffusion rate in the intermetallic itself that would be the short-circuit. Of course, cracks and pores are not present only in the vicinity of intermetallics [12]. Observing hydrogen concentrations in an intermetallic after cooling to room temperature is no more evidence that it was present there during oxidation than is the observation of hydrogen concentrated in the Zr layer of barrier cladding during PIE observations [21].

The chemical exchange experiments show that ionic species are able to move relatively freely in and out of pores or cracks, even in pre-transition oxide films, and that the critical process in terms of hydrogen absorption could be occurring at the bottom of such features. During post-transition oxidation it has been shown that the hydrogen uptake rates decrease when the solubility of hydrogen (TSS) in the metal is exceeded [5,22]. The decrease in the hydrogen uptake rate after exceeding TSS has been explained as a result of hydride precipitation at the oxide/metal interface at the bottom of pores or cracks that penetrate to this point [5]. In order to force hydrogen to precipitate as a solid layer at the metal surface in zirconium alloys (in the absence of a temperature gradient) a very high local ingress rate is required. A comparison of this rate with the average rate of ingress through post-transition oxides suggests that about 10^{-4} of the oxide/metal interface is active as a location for hydrogen absorption at any point in time [5].

Since the exchange experiments suggest a small number of pores or cracks to be present in pre-transition oxides [4], and electron microscopy has shown examples of these [12,13,18], it was of interest to see whether a change in hydrogen uptake rate could be observed when TSS was exceeded during pre-transition oxidation. This would indicate that the same hydrogen uptake process was occurring as in post-transition oxidation. For TSS to be exceeded after <2 μm oxide growth the specimens would need to be very thin, and a 0.125 mm thick sheet of Zircaloy-2 was available. This paper reports results for hydrogen uptake during pre-transition oxidation in steam of specimens from this sheet.

2. Experimental

A batch of very thin Zircaloy-2 sheet (0·125 mm), supplied by Imperial Metal Industries (UK), was available for this study. Because only one thickness of sheet was used, the previous technique of looking for departures of the hydrogen uptake rate of thin specimens from those of thicker specimens could not be adopted. It was necessary to rely on identifying departures of the hydrogen uptake kinetics from a fixed relationship to the concurrent oxidation kinetics curve. In the pre-transition region the oxidation kinetics in steam are close to cubic, but with at least one significant inflection to complicate the analysis [25]. In order to demonstrate a change in the hydrogen absorption kinetics, therefore, a large number of data points would be needed, and the hydrogen analysis should be free of excessive scatter. This could be achieved by using large area specimens for both oxidation and hydrogen analyses. The study was rendered more difficult by the high initial hydrogen content of the sheet (average ~40 ppm). This could have been accommodated easily if it had been uniform, however, it soon became evident that it varied from position to position in the sheet from 30–60 ppm. In order, to eliminate as much error as possible in this study, therefore, large numbers of control analyses were needed. Nevertheless, the total quantity of hydrogen being extracted from these samples was near the minimum for acceptable analyses, so that scatter could not be avoided.

The very thin sheets employed to minimise the errors in the oxidation and hydrogen uptake determinations required different treatments in order to cover the various weight gain ranges (roughly 0–5; 5–30 mg/dm^2). Specimens were prepared in separate batches of 10–12 specimens, and these batches can be identified from the contiguous specimen numbers given in Table 1. Blanks for hydrogen analysis were prepared in several different ways. If it was intended to oxidise the specimens to <30

mg/dm^2, one specimen from each batch was cut up after the final chemical polishing specimen preparation step and analysed for hydrogen to provide the blank correction; if the intended weight gains were <5 mg/dm^2, one piece was cut from each end of each specimen after specimen preparation and analysed for hydrogen. Samples were thin enough that the sheet could be cut with a sturdy pair of scissors. These ranges were not strictly adhered to, firstly, because of the difficulties in predicting the specimen weight gain before exposure and, secondly, because it only became evident that there were big local variations in the initial hydrogen in the thin sheet during the experiments, and hence as time went on the tendency was to cut blanks from every specimen. Hydrogen analyses of specimens were done in duplicate in all instances and, where large variations in H content with position in the oxidised specimen were found, additional analyses were performed. Hydrogen analysis was by hot vacuum extraction at 1300°C with intermediate blank determinations, and an error of ±5 ppm is possible for low hydrogen contents increasing to ±5% at higher values (>100 ppm). While many of the specimens showed about this amount of variability, Table 1 shows that a number had larger scatter.

The specimens from each group (final size 1×4 cm) were inserted in the 1 atm. steam furnace at the same time and were removed one at a time at predetermined intervals for weighing and analysis. No specimens were replaced in the furnace, so that each had one oxidation exposure of the length indicated in Table 1. The specimens underwent small temperature cycles as the furnace was opened to remove each individual specimen and then immediately closed again. The steam flow was high enough to minimise the disturbance that each specimen removal caused.

3. Results

The hydrogen analyses obtained in this study are tabulated in Table 1 for the temperatures of 300°C, 350°C and 400°C. Data obtained in 500 psi (3.5 MPa) steam and water vapour (svp at room temperature) are also presented for completeness. These specimens were oxidised in silica ampoules and a Sartorius vacuum balance respectively. The former are in general agreement with the 1 atm. data, but were available only at 300°C and are fewer in number than the 1 atm. data. The latter were also fewer in number than the 1 atm. data. Data in moist air (not presented) were few, and the TSS was reached in this environment only close to the oxidation rate transition. One result of this was the remaining doubts about the extent of porosity in the oxide associated with the moist air data. The analysis of the material is given in Table 2, and a two-stage Formvar-carbon electron micrograph of a specimen surface after preparation is shown in Fig. 1.

The oxygen weight gains (with the weight of absorbed hydrogen subtracted) and the total hydrogen contents of the specimens are plotted for 300°C, 350°C and 400°C in Figs. 2–4. Smooth curves have been drawn through the oxidation data. Evidence for a plateau in these curves at ~10 mg/dm^2 weight gain was much less than previously reported [25]. However, there was much scatter in the 300°C curve at about this point, and a similar anomaly in the 350°C and 400°C data at about the same point. These curves were used to calculate hydrogen uptake curves for constant percentage uptakes for the initial stage of oxidation that represent upper and lower bound percentages or an approximate mean for the hydrogen uptake data depending on the extent of the scatter. The hydrogen contents departed from these limiting curves towards a lower percentage uptake curve at higher weight gains. A second fixed percentage uptake curve was then drawn to give a fit to the hydrogen contents of the highest weight gain specimens in the set, and this curve (or curves) was extended back until it intersected the first curve (or curves). The change from one set of hydrogen uptake curves to another was taken as an indication of a reduction in the rate of hydrogen absorption from one percentage uptake to a lower one, and the intersections of the two sets of curves defined the hydrogen contents at which this change in percentage uptake occurred.

The numerical values obtained from this interpretation have been plotted on recent curves of TSSD (dissolution) and TSSP (precipitation) in Fig. 5 [26]. It can be seen that the agreement with these results is very good at 300°C and 350°C, but that at 400°C the change in percentage uptake appears to occur at a hydrogen content somewhat below the expected range for hydrogen solubility data obtained during the hydride precipitation process. The recent data for the cooling curves reveal two separate stages of hydride precipitation (TSSP1 and TSSP2) and the 400°C data are close to the lowest reported values (TSSP2) obtained from the cooling curves [26].

4. Discussion

Despite the best attempts, the scatter on the resulting data was larger than had been hoped for. So the first consideration must be whether the interpretation of the hydrogen uptake curves in terms of two periods; (an early high percentage uptake and a later low percentage uptake) is valid. There is no doubt that the percentage hydrogen uptake had decreased from the start of oxidation to the beginning of the kinetic rate transition (~2 μm), however, whether the results are better interpreted as a smoothly decreasing percentage uptake curve or a

Table 1
Hydrogen uptake data

Specimen number	Environment	Time (days)	Wt. Gain (mg/dm^2)	Initial H content (ppm)	Final H content (ppm)	ΔO (mg/dm^2)	ΔH (mg/dm^2)
A. ICI Zr-20 at 300° C							
I1	1 atm steam	1.0	2.885	43	81,92	2.680	0.179; 0.231
I2	1 atm steam	2.0	5.7243	43	105,110	5.427	0.282; 0.305
13	1 atm steam	3.0	7.181	43	115,125	6.830	0.325; 0.380
I4	1 atm steam	4.0	7.695	43	110,120	7.365	0.297; 0.364
I5	1 atm steam	5.0	7.280	43	115,120	6.960	0.312; 0.334
I6	1 atm steam	8.0	8.780	43	120,125	8.430	0.341; 0.364
I7	1 atm steam	12.0	10.67	43	130,130	10.29	0.384; 0.384
I8	1 atm steam	16.0	9.876	43	120,120	9.540	0.338; 0.338
I9	1 atm steam	21.0	11.45	43	150,170	10.95	0.465; 0.553
I10	1 atm steam	28.0	10.90	43	150,150	10.43	0.472; 0.472
I11	1 atm steam	47	14.43	43	175,195	13.79	0.590; 0.680
I12	1 atm steam	122	16.00	43	170,170	15.40	0.585; 0.585
I13	1 atm steam	0.33	0.872	34	68,75	0.750	0.112; 0.133
I14	1 atm steam	0.66	2.450	34	74,78	2.260	0.200; 0.182
I15	1 atm steam	1.33	3.960	34	90,98	3.730	0.211; 0.247
I16	1 atm steam	1.66	4.800	34	89,93	4.535	0.274; 0.255
I17	1 atm steam	0.33	1.001	52.5	59,62	0.966	0.029; 0.043
I18	1 atm steam	0.66	2.778	42	71,76	2.634	0.133; 0.155
I19	1 atm steam	1.0	3.602	44.5	80,86	3.428	0.161; 0.189
I20	1 atm steam	1.33	3.710	50	96,100	3.530	0.176; 0.191
I21	1 atm steam	1.66	4.841	59.5	89,93	4.660	0.167; 0.184
I22	1 atm steam	2.00	6.220	51.5	100,110	5.930	0.260; 0.314
I28	1 atm steam	0.021	0.07	58.5	65,68	0.04	0.025; 0.037
I29	1 atm steam	0.083	0.206	38.5	49,50	0.160	0.041; 0.047
I30	1 atm steam	0.125	0.341	38.5	55,58	0.270	0.063; 0.075
I31	1 atm steam	0.166	1.307	38.5	57,63	0.957	0.070; 0.093
I32	1 atm steam	0.312	1.415	38.5	65,72	1.305	0.098; 0.125
I34	1 atm steam	0.500	2.100	38.5	71,79	1.965	0.119; 0.148
I35	1 atm steam	0.66	2.576	38.5	85,87	2.409	0.163; 0.170
I36	1 atm steam	1.00	3.471	38.5	86,96	3.330	0.161; 0.195
I23	Water vap. (SVP)	6.0	6.66	43	130,140	6.27	0.368; 0.410
I24	Water vap. (SVP)	0.25	0.70	43	43,50	0.67	0.00; 0.029
I38A	Water vap. (SVP)	10.0	9.63	43	170,180	9.09	0.522; 0.563
I54	500 psi steam	0.33	3.691	36	110,120	3.330	0.333; 0.378
I55	500 psi steam	0.33	3.119	36	88,88	2.880	0.232; 0.232
I56	500 psi steam	0.66	6.816	36	105,105	6.520	0.293; 0.293
I57	500 psi steam	0.66	6.491	36	110,110	6.160	0.329; 0.329
I58	500 psi steam	1.0	3.098	36	47,47	3.050	0.049; 0.049
I59	500 psi steam	1.0	3.130	36	59,59	3.020	0.108; 0.108
I60	500 psi steam	2.0	6.850	36	89,91	6.610	0.237; 0.246

Table 1 (Continued)

Specimen number	Environment	Time (days)	Wt. Gain (mg/dm^2)	Initial H content (ppm)	Final H content (ppm)	ΔO (mg/dm^2)	ΔH (mg/dm^2)
I61	500 psi steam	2.0	6.660	36	91,93	6.410	0.246; 0.255
I103	500 psi steam	1.0	6.45	41	170,190	5.7	0.720; 0.832
I104	500 psi steam	1.0	6.45	38	150,150	5.8	0.755; 0.755
I105	500 psi steam	2.0	12.7	36	160,165	12.1	0.540; 0.562
I106	500 psi steam	2.0	8.05	36	165,180	7.40	0.577; 0.644
I107	500 psi steam	7.0	14.48	36	170,185	13.86	0.578; 0.612
I108	500 psi steam	7.0	13.36	36	170,170	12.78	0.585; 0.585
I109	500 psi steam	14.0	16.68	43	155,185	16.12	0.500; 0.633
I110	500 psi steam	14.0	14.45	43	185,185	13.91	0.540; 0.540
B. ICI Zr-20 at 350° C							
I37	1 atm steam	0.083	3.90	40	85,90	3.69	0.202; 0.224
I38	1 atm steam	0.166	4.12	40	95,105	3.86	0.242; 0.286
I39	1 atm steam	0.250	4.53	40	100,110	4.25	0.268; 0.314
I40	1 atm steam	0.333	5.31	40	100,120	5.00	0.267; 0.356
I41	1 atm steam	0.50	5.55	40	100,110	5.27	0.263; 0.307
I42	1 atm steam	0.666	6.47	40	120,130	6.10	0.351; 0.395
I43	1 atm steam	1.0	7.69	40	110,120	7.36	0.309; 0.353
I44	1 atm steam	1.5	9.76	40	130,130	9.35	0.407; 0.407
I45	1 atm steam	2.0	9.505	40	120,130	9.11	0.376; 0.412
I46	1 atm steam	3.0	13.30	40	150,160	12.78	0.500; 0.547
I47	1 atm steam	5.0	17.40	40	170,170	16.74	0.665; 0.665
I48	1 atm steam	7.0	18.40	40	190,200	17.70	0.683; 0.730
I49	1 atm steam	1.0	24.00	40	220,230	23.18	0.80; 0.84
I52	1 atm steam	21	30.68	36	330,330	29.34	1.34; 1.34
I64	1 atm steam	0.0104	0.345	36	60,62	0.240	0.104; 0.113
I65	1 atm steam	0.0208	0.575	36	55,61	0.485	0.082; 0.108
I66	1 atm steam	0.0417	1.441	36	62,66	1.320	0.112; 0.129
I67	1 atm steam	0.125	3.611	36	105,105	3.310	0.300; 0.300
I68	1 atm steam	0.333	5.500	36	170,185	4.900	0.580; 0.640
I69	1 atm steam	0.583	7.270	36	120,130	6.900	0.360; 0.403
I70	1 atm steam	0.833	8.251	36	120,140	7.850	0.356; 0.440
I71	1 atm steam	1.5	10.216	36	160,165	9.69	0.515; 0.536
I72	1 atm steam	2.5	12.316	36	175,175	11.76	0.557; 0.557
I139	1 atm steam	7	19.54	30	190,190	18.84	0.70; 0.70
I140	1 atm steam	14	28.09	45	260,300	26.97	1.03; 1.22
I141	1 atm steam	28	38.89	29	310,310	37.60	1.29; 1.29
I142	1 atm steam	42	48.9	36	500,520	46.7	2.12; 2.22
I143	1 atm steam	56	40.5	36	370,410	39.0	1.45; 1.62
I144	1 atm steam	84	49.6	36	530,590	47.0	2.71; 2.42
I145	1 atm steam	112	48.7	36	360	47.6	1.61
I146	1 atm steam	143	48.0	36	480,500	45.9	2.02; 2.12

Table 1 (Continued)

Specimen number	Environment	Time (days)	Wt. Gain (mg/dm^2)	Initial H content (ppm)	Final H content (ppm)	ΔO (mg/dm^2)	ΔH (mg/dm^2)
I53	Water vap.	3	15.3	36	150,160	14.8	0.48; 0.52
C. ICI Zr-20 at 400°C							
I83	1 atm steam	0.0104	2.433	36	45,52	2.390	0.041; 0.068
I84	1 atm steam	0.0208	3.151	30	61,71	2.980	0.156; 0.188
I85	1 atm steam	0.0313	3.588	29	74,81	3.367	0.205; 0.237
I86	1 atm steam	0.0417	3.765	42	82,85	3.580	0.180; 0.194
I87	1 atm steam	0.0625	4.540	38	86,87	4.320	0.220; 0.224
I88	1 atm steam	0.0833	4.899	33	89,90	4.647	0.249; 0.254
I89	1 atm steam	0.125	6.490	31	105,105	6.150	0.337; 0.337
I90	1 atm steam	0.166	6.100	31	98,99	5.800	0.297; 0.300
I91	1 atm steam	0.207	7.560	36	105,110	7.240	0.311; 0.332
I92	1 atm steam	0.250	8.360	36	105,105	8.010	0.350; 0.350
I93	1 atm steam	0.292	7.500	36	105,115	7.170	0.310; 0.355
I94	1 atm steam	0.333	8.160	36	100,110	7.840	0.290; 0.336
I95	1 atm steam	0.500	11.420	36	120,130	11.040	0.363; 0.407
I96	1 atm steam	0.750	13.80	36	150,150	13.30	0.505; 0.505
I97	1 atm steam	1.00	17.30	36	150,160	16.76	0.51; 0.56
I98	1 atm steam	2.00	21.82	36	180,190	21.14	0.66; 0.70
I99	1 atm steam	3.00	21.29	36	170,190	20.64	0.60; 0.69
I100	1 atm steam	5.00	25.80	36	200,220	25.01	0.74; 0.83
I101	1 atm steam	7.00	31.40	36	230,240	30.48	0.89; 0.935
I102	1 atm steam	10	33.50	36	250,250	32.51	0.99; 0.99
I147	1 atm steam	7.00	36.80	46	310,320	35.60	1.17; 1.22
I148	1 atm steam	14	46.20	48	430,460	44.50	1.67; 1.81
I149	1 atm steam	21	55.6	36	760,810	52.5	3.05; 3.26
I150	1 atm steam	28	76.6	32	690,740	73.6	2.85; 3.07
I151	1 atm steam	35	88.2	36	1100,1100	83.6	4.63; 4.63
I152	1 atm steam	42	97.5	36	1350,1400	92.0	5.6; 5.8
I153	1 atm steam	49	106.0	36	1200,1400	100	5.2; 6.1
I154	1 atm steam	56	125.5	36	1300,1400	119.5	5.85; 6.33
I73	Water vap. (SVP)	2.0	26.5	36	210,220	25.7	0.79; 0.83

Table 2
Manufacturer's analysis of IMI Zircaloy-2 sheet

Sn (wt.%)	1.58
Fe (wt.%)	0.12
Cr (wt.%)	0.09
Ni (wt.%)	0.05
O (ppm/wt.)	1650
H (ppm/wt.)	40 [a]
N (ppm/wt.)	100
C (ppm/wt.)	120
Si (ppm/wt.)	65
Hf (ppm/wt.)	270
Ti (ppm/wt.)	5
Al (ppm/wt.)	117

[a] For H analyses of actual specimens see Table 1.

two-stage one is difficult to decide. At 300°C (Fig. 2) a relatively sharp discontinuity at ~0.5 μm oxide thickness appears probable. At 350°C (Fig. 3) the scatter was significantly worse, and a sharp change in percentage uptake is less clearly discernible. At 400°C (Fig. 4) plotting the pre-transition data only (to avoid confusion with the onset of the oxidation rate transition) a two-stage hydrogen uptake process remains probable, although the reduction in percentage uptake is much diminished.

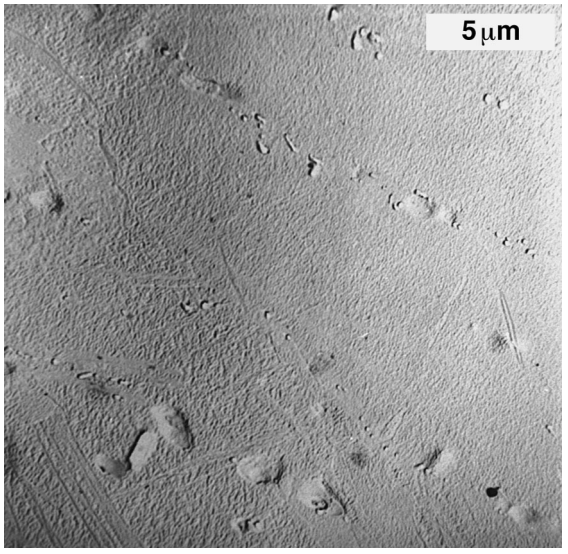

Fig. 1. Replica electron-micrograph (Formvar-carbon, Au/Pd shadowed) of a chemically polished surface of Zircaloy-2 sheet. Note the alignment of the second-phase particles. The small round particles (0.2–0.4 μm) are probably $Zr(Fe/Cr)_2$. The small elongated particles may be either zirconium silicide or carbide, and the large round or oval pits (1–2 μm) were left when $Zr_2(Fe/Ni)$ particles were dissolved by the chemical polishing solution. The maximum particle size would be smaller than the pit dimensions.

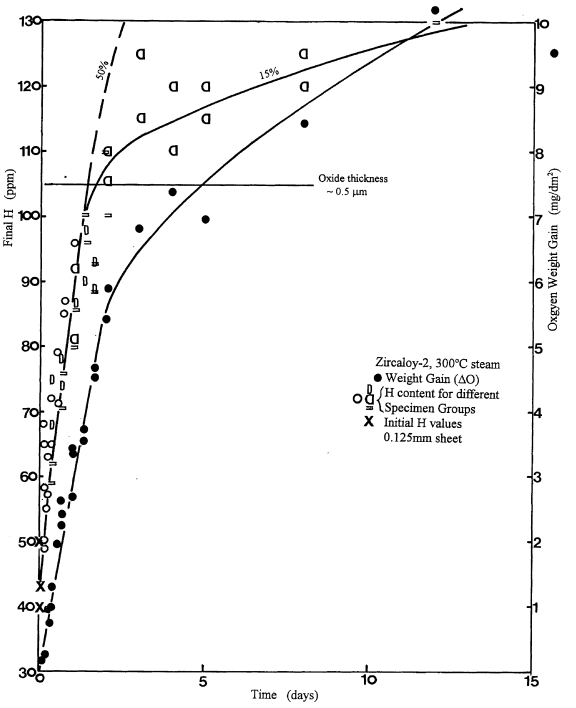

Fig. 2. Oxygen weight gain and hydrogen content plots for 0.125 mm thick Zirc-20 sheet in 300°C (573 K) steam at 100 kPa. The different symbols for hydrogen contents are for different groups of specimens prepared, oxidised and analysed at the same time.

If there were theoretical grounds for expecting a smooth change in percentage uptake during pre-transition oxidation then the results would not be sufficiently clear to overturn such an expectation. However, only a mechanism based on hydrogen diffusion through the whole of the oxide thickness via oxide crystallite boundaries would appear to be capable of generating such a curve [2]. The predominance of oxygen diffusion along oxide crystallite boundaries and the decreasing crystallite boundary area, as the oxide thickens, have been argued to be the causes of the approximately cubic (rather than parabolic) pre-transition oxidation kinetics [27,28]. If both hydrogen and oxygen are diffusing through the film via the same crystallite boundaries then both weight gain and hydrogen uptake curves should follow the same kinetics. However, an earlier study [29] of the initial oxidation of Zircaloy-2 at 300°C showed that a better fit could be obtained to a log/linear plot (except at very short times) than to a log/log plot. The 300°C data from this study and those from reference 28 were plotted in this form (Fig. 6). It can be seen that both give excellent straight lines for exposures longer than about 12 h. The data for the 0.125 mm thick specimens are more scattered because every point is from an individual specimen that was oxidised only once

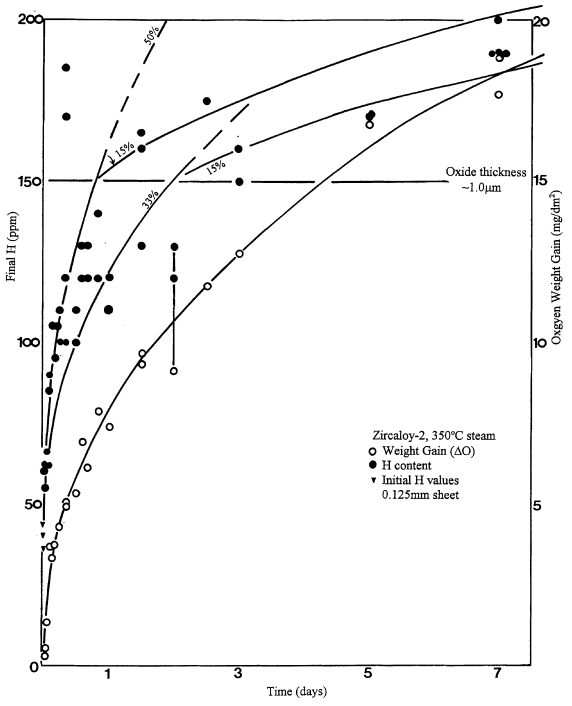

Fig. 3. Oxygen weight gain and hydrogen content plots for 0.125 mm thick Zirc-20 sheet in 350°C (623 K) steam at 100 kPa.

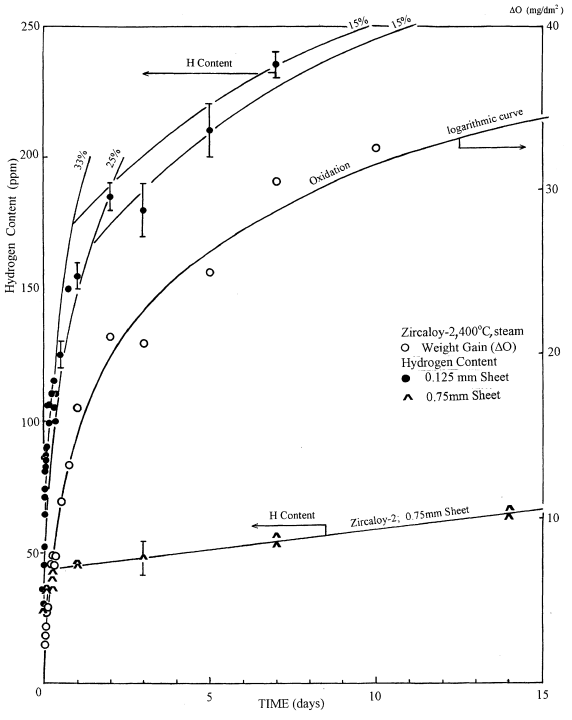

Fig. 4. Oxygen weight gain and hydrogen contents plots for 0.125 mm thick Zirc-20 sheet, and hydrogen content data for a similar 0.75 mm thick sheet in 400°C (673 K) steam at 100 kPa.

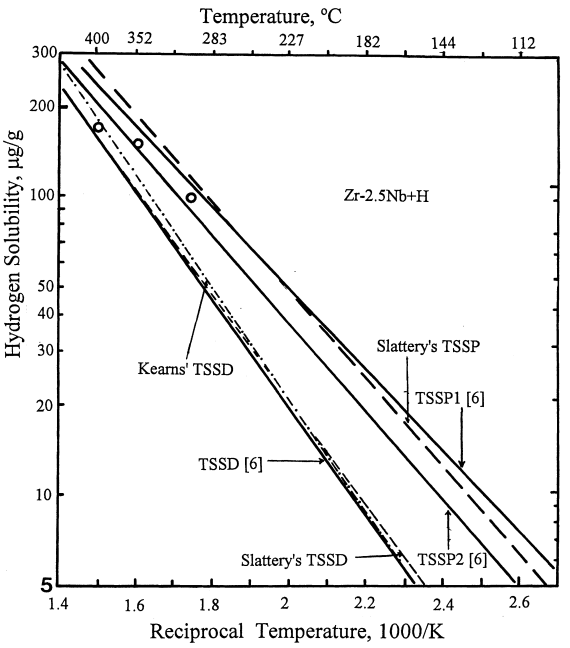

Fig. 5. A comparison of the hydrogen contents at which decreases in hydrogen uptake rates for 0.125 mm thick sheet were observed with recent data for hydrogen solubility from Ref. [26].

for the indicated time, but the scatter is comparable to that for the other data [28] which were for large specimens; were averages of eight specimens; and all were oxidised and weighed discontinuously during the complete experiment after each autoclave cycle. No inflec-

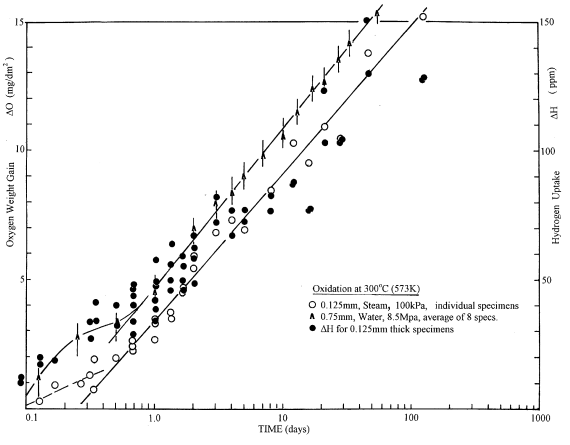

Fig. 6. Oxidation kinetics at 300°C (573 K) for 0.125 and 0.75 mm sheets of Zircaloy-2 on a log/linear plot. The hydrogen uptake data are also plotted. Note the linearity of the oxidation kinetics in the critical range of 3–15 mg/dm^2. The hydrogen uptake follows the oxidation kinetics up to 7 mg/dm^2 when a sharp decrease in uptake rate is seen.

tion, such as that observed in the water data, was observed here. The goodness of the fit to a single logarithmic rate equation indicates that one oxide growth mechanism persisted throughout that time period, so that no discontinuity in the hydrogen uptake kinetics because of a change in oxidation kinetics can be justified in the region where the reduction in percentage uptake appears to occur. When the hydrogen uptake figures were plotted on the same logarithmic kinetic plot they paralleled the oxidation kinetics nicely up to an oxide thickness of 0.5 μm when they suddenly dropped below the kinetic line suggesting a sudden reduction in the uptake kinetics at this point. This suggests that the interpretation of the H uptake as a two-stage process is the correct one.

Logarithmic oxidation kinetics are generally thought to be largely controlled by the electric field in the oxide [30], and the field across the oxide in zirconium alloys has been shown to have a negative potential on the base metal that decreases after a few hours (where the inflection in the oxidation curve is) as the oxide thickens. The potential then remains relatively constant [31]. Thus, the electric field across the oxide will be decreasing steadily as the oxide thickens. If the hydrogen uptake process were controlled by the diffusion of protons through the oxide (either through the bulk or at the crystallite boundaries [2]) then the driving force would decrease as the oxide thickens and the hydrogen uptake rate might also be expected to decrease. This would be a smooth decrease if the field decreased smoothly, but might decrease suddenly if the field did the same. Since the inflections in the oxidation and hydrogen uptake curves do not coincide, the drop in electrical potential on the metal cannot explain the drop in H uptake rate [31].

Hydrogen uptake data for some 0.75 mm thick Zircaloy-2 specimens oxidised in 400°C steam have been plotted in Fig. 4 [22]. Because of the higher specimen thickness all the hydrogen contents are well below TSS and no change in uptake rate at an oxide thickness corresponding to the change in H uptake in thin specimens is seen. What is observed is a rapid initial hydrogen uptake, during the growth of the first few tenths of a micron of oxide, which then falls to a much lower (but linear) uptake rate before the oxide reaches 0.5 μm. This corresponds to the region of initial oxide film growth where tritium diffusion out of an initially tritided specimen was significant (Fig. 7), but diminishing rapidly with increasing oxide thickness [32]. This has been explained as resulting from hydrogen (tritium) escaping through flaws (in the initial oxide on the specimen) which are passivating during the growth of the thin oxide film. The continued escape of tritium (from ternary fission in the UO_2) through the fuel cladding in light water reactors, for which only anecdotal evidence is currently available [33], shows that some flaws in the

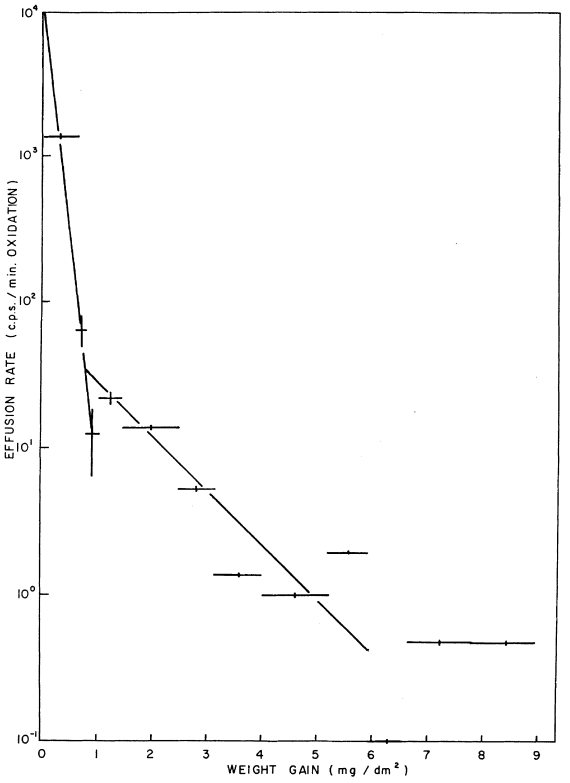

Fig. 7. Tritium effusion from pre-tritided zirconium specimens during oxidation in oxygen at 400°C (673 K) [32].

oxide film continue to be present throughout the oxidation process. Easy exchange of tritium for hydrogen at "bare-metal" sites in the oxide film probably explains the observation that tritium effusion was two orders of magnitude faster when tritided specimens were oxidised in steam (H_2O) than when the specimens were oxidised in oxygen, as in Fig. 7 [32].

Thus, there would seem to be ample evidence for a small number of flaws in zirconium oxide films through which hydrogen atoms can enter (or leave) the metal directly depending upon the chemical conditions within these flaws, with the numbers of flaws varying throughout the oxidation curve, but never actually vanishing.

The electric field across the oxide would be equally as important as the internal chemistry if protons are migrating down small cracks or pores (or along the surfaces of such flaws), the key to understanding these hydrogen uptake results, therefore, is some independent knowledge of whether the process is general or local; and if local at which sites on the specimen surface. In a recent study of cathodic sites in anodic oxide films on Zircaloy-2 [34], the technique involved cathodically polarising the specimens in a dilute $CuSO_4$ solution to deposit small Cu balls on the active cathodic sites; lo-

cating these balls by scanning electron microscopy, and identifying the cathodic site by the same technique after dissolving the Cu. When this technique was applied here to a Zircaloy-2 specimen oxidised in 300°C steam. The results (Fig. 8) showed a small number of active cathodic sites (~50 per mm^2) and all the sites examined proved to be small cracks in the surface oxide. None of them were at the sites of $Zr(Fe/Cr)_2$ intermetallics that were present in the original specimen surface, but the largest Cu balls were at cracks around etch pits left by dissolving $Zr_2(Fe/Ni)$ intermetallics during surface preparation [34,35].

If we assume an area of 0.05 μm^2 for each active site; ~50 sites/mm^2; then, if the number and size of sites remains the same at temperature, for the total hydrogen absorption rate of 1.2×10^{-5} μg (H) cm^{-2} s^{-1} observed

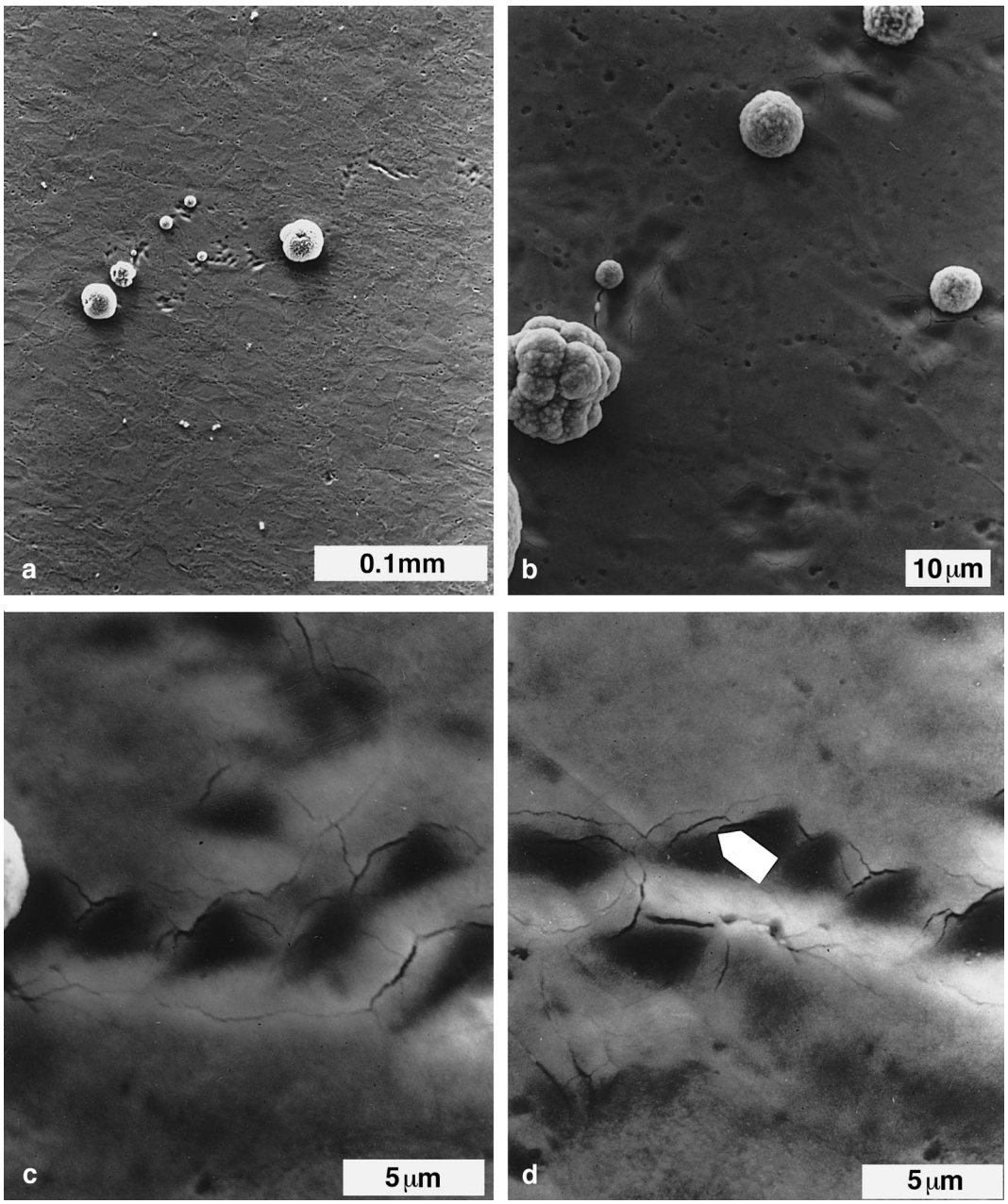

Fig. 8. Scanning electron-micrographs of Cu deposited cathodically on an oxidised Zircaloy-2 surface (1.2 μm oxide). (a) Distribution of large and small Cu balls on the surface. (b) Group of large balls from (a). (c) Crack pattern in oxide adjacent to RH ball in (b). (d) Nucleation site for this ball (arrowed).

at 300°C before the decrease in uptake rate, the local hydrogen flux at an average individual site would be ~5 μg cm^{-2} s^{-1}. This is much higher than the hydrogen flux needed to form solid hydride layers on Zircaloy surfaces (2×10^{-3} μg cm^{-2} s^{-1}) during corrosion in concentrated LiOH solutions at 300°C [5].

With evidence accumulating that H uptake is taking place at flaws rather than by diffusion through the bulk of the oxide, it is possible to speculate on what the micromechanism for hydrogen uptake at the bottom of a small pore or crack in the oxide might be. If the current concept of the barrier film on zirconium alloys is correct (i.e. that it is the time averaged value of the boundary marking the loci of points of closest approach of small pores or cracks to the oxide/metal interface) then cracks or pores are propagating right up to this interface, at least transiently [23,24]. The sequence of events following the arrival of such a small crack or pore at the interface should be considered. Initially, if the pore is filled with steam or water this will immediately react with the metal at the bottom of the pore to reform an oxide film. Little of the hydrogen may be absorbed during this process [36]. Then hydrogen which is not immediately absorbed will accumulate at the bottom of the pore since (at least in steam) there will be no pressure drop when a molecule of water is converted to oxide and a molecule of hydrogen. By this process it would be possible to produce a small region of relatively pure hydrogen at the bottom of the pore if interdiffusion along the pore is slow compared to the other processes. It is possible to conceive of a microscopic "steam depletion" region being generated at the bottom of the pore [37]. Thus, after an incubation period (that allows for oxide breakdown at the bottom of the pore) the hydrogen remaining in the bubble will be absorbed by the metal. This allows access of more water molecules to the interface, thus repassivating the surface and restarting the "steam depletion" cycle.

The percentage hydrogen uptake that is observed would then be determined by the fraction of the corrosion hydrogen remaining in the hydrogen bubble at the time when the oxide at the bottom of the pore breaks down. The rest of the corrosion hydrogen would be lost by back diffusion out of the pores. Thus, the geometry of the pores in the oxide film should be important in determining the uptake percentage. This may be the factor which is affected by the precipitate size and composition in the alloy [14].

5. Conclusions

Analysis of hydrogen uptake data from very thin Zircaloy-2 specimens where the terminal solid solubility of hydrogen in the zirconium matrix was reached during the pre–transition oxidation period in steam at 300–400°C showed that the hydrogen uptake kinetics changed (the rate of uptake decreased) when TSS was reached. This is interpreted to mean that the uptake process was so local that the uptake rate at the uptake site was high enough to precipitate hydrogen at the entry site. This translates into an active surface site area fraction for the hydrogen uptake process during pre-transition oxidation of $\sim 2 \times 10^{-6}$; much smaller than the active area calculated during post-transition oxidation [5]. This cannot be correlated with intermetallic particle properties, since all specimens were pickled, thus removing all Zr_2(Fe/Ni) particles from the initial surfaces. The sites were observed to be small cracks or pores that develop in the oxide film even during pre-transition oxidation and were not apparently associated with second-phase particles. A mechanism that is basically a microscopic version of a "steam depletion" process for hydrogen absorption occurring at the bottom of a small pore or crack is proposed for the hydrogen absorption process during corrosion. In such a mechanism the geometry and frequency of flaws or cracks in the oxide would be a critical factor. These may be influenced by factors such as precipitate size distribution which have already been correlated with hydrogen uptake rates [14].

References

[1] M.B. Elmoselhi, J. Alloys Comp. 231 (1995) 716.
[2] Y. Hatano, K. Isobe, R. Hitaka, M. Sugisaki, J. Nucl. Sci. Tech. 33 (1996) 944.
[3] M.B. Elmoselhi, B.D. Warr, S. McIntyre, ASTM-STP1245, 1994, 62.
[4] N. Ramasubramanian, Lithium and boron effects in the corrosion mechanism of zirconium alloys under coolant chemistry conditions, in: Proceedings of the seventh BNES Conference on Water Chemistry of Nuclear Reactor Systems, Vol. 1, Bournemouth, UK, 1996, p. 91.
[5] B. Cox, J. Alloys Comp. 256 (1997) 244.
[6] D. Khatamian, F.D. Manchester, J. Nucl. Mater. 166 (1989) 300.
[7] D. Khatamian, Z. Phys. Chem. 18 (1993) 435.
[8] D. Khatamian, J. Alloys Comp. 253&254 (1997) 471.
[9] N.S. McIntyre, C.G. Weisener, R.D. Davidson, W.N. Lennard, G.R. Weisener, I.V. Mitchell, A. Brennenstuhl, B.D. Warr, Surf. Interface Anal. 15 (1990) 591.
[10] N.S. McIntyre, R.D. Davidson, C.G. Weisener, G.M. Good, G.R. Mount, B.D. Warr, M. Elmoselhi, J. Vac. Sci. Technol. A9 (1991) 1402.
[11] H.-J. Beie, A. Mitwalsky, F. Garzarolli, H. Ruhmann, H.-J. Sell, ASTM-STP-1245, 1994, p. 615.
[12] R.A. Ploc, S.B. Newcomb, Porosity in zirconium oxide films, in: Proceedings of the 3rd International Conference on the Microscopy of Oxidation, 16–18 September 1996, Inst. of Materials, UK.
[13] D. Pecheur, J. Godlewski, P. Billot, J. Thomazet, ASTM-STP-1295, 1996, p. 94.

[14] K. Isobe, Y. Hatano, M. Sugisaki, J. Nucl. Mater. 248 (1997) 315.
[15] B. Cox, M.J. Davies, A.D. Dent, Hydrogen absorption during oxidation in steam and aqueous solutions, UK Report, AERE-M621, 1960, U.K.A.E.A., Harwell, Berks.
[16] B. Cox, The effect of some alloying additions on the oxidation of zirconium in steam, UK Report, AERE-R4458, 1963, U.K.A.E.A., Harwell, Berks.
[17] J. Godlewski, ASTM-STP-1245, 1994, p. 663.
[18] B. Cox, M. Ungurelu, Y.-M. Wong, C. Wu, ASTM-STP-1295, 1996, 114.
[19] B. de Gélas, G. Béranger, P. Lacombe, J. Nucl. Mater. 28 (1968) 185.
[20] B. Cox, H.I. Sheikh, J. Nucl. Mater. 249 (1997) 17.
[21] M. Nakatsuka, M.Sc.T. Torimaru, Internal hydriding of irradiated zirconium liner and non-liner Zry-2 tubes, in: Proceedings of the BNES TopFuel'97 Conference, Manchester, UK, p. 2.73.
[22] B. Cox, J. Electrochem. Soc. 109 (1962) 6.
[23] B. Cox, J. Less Common Met. 5 (1963) 325.
[24] J.N. Wanklyn, C.E. Britton, D.R. Silvester, N.J.M. Wilkins, J. Electrochemical Soc. 110 (1963) 856.
[25] B. Cox, J. Nucl. Mater. 25 (1968) 310.
[26] Z.L. Pan, I.G. Ritchie, M.P. Puls, J. Nucl. Mater. 228 (1996) 227.
[27] B. Cox, J.P. Pemsler, J. Nucl. Mater. 28 (1968) 73.
[28] B. Cox, Oxidation of Zirconium and its alloys, Advances in Corrosion Science and Technology, M.G. Fontana, R.W. Staehle (Eds.), Vol. 5, Plenum Press, NY ,1976, p. 173.
[29] B. Cox, J. Electrochem. Soc. 108 (1961) 24.
[30] IAEA-TECDOC 996, Waterside Corrosion of Zirconium Alloys in Nuclear Power Plants, International Atomic Energy Agency, Vienna, 1998.
[31] B. Cox, J. Nucl. Mater. 31 (1969) 48.
[32] B. Cox, C. Roy, The use of tritium as a tracer in studies of hydrogen uptake by zirconium alloys, Canadian Report, AECL-2519, 1965.
[33] C. Lemaignan, CENG Grenoble, Private communication.
[34] B. Cox, F. Gauducheau, Y.-M. Wong, J. Nucl. Mater. 189 (1992) 362.
[35] B. Cox, J. Nucl. Mater. 29 (1969) 50.
[36] D.W. Freer, D.R. Silvester, J.N. Wanklyn, Corrosion 21 (1965) 137.
[37] D.R. Olander, W.-E. Wang, Y. Kim, C.Y. Li, S.K. Yagnik, Investigation of the Roles of Corrosion and Hydriding of barrier Cladding and Fuel Pellet Oxidation in BWR Fuel Degradation, in: Proceedings of the ANS International Topical Meeting on Light Water Reactor Fuel Performance, Portland, OR, March 1997, p. 149.